PERGAMON International Journal of Engineering Science 37 (1999) 1369–1387

International Journal of Engineering Science

Guided circumferential waves in layered cylinders

Christine Valle [a], Jianmin Qu [a,*], Laurence J. Jacobs [b]

[a] *The George W. Woodruff School of Mechanical Engineering, Georgia Institute of Technology, Atlanta, GA 30332-0405, USA*

[b] *School of Civil and Environmental Engineering, Georgia Institute of Technology, Atlanta, GA 30332, USA*

Received 23 July 1998; accepted 22 September 1998

Abstract

This paper examines the propagation of time harmonic circumferential waves in a two-dimensional (infinitely long) hollow cylinder with an inner shaft. The boundary condition at the interface (between the inner shaft and the outer cylinder) is assumed as free-sliding; that is, the interfacial shear stresses are assumed to be zero, and the normal stress and radial displacements are continuous. The dispersion relationship is obtained from linear elasticity theory, and numerical results for the dispersion curves of the first several modes are presented. In addition, displacement profiles along the radial directions are provided. These results show that, at higher frequencies, the first mode asymptotically tends to a Rayleigh wave on a flat surface, while the second mode also approaches a Rayleigh wave propagating along the free-sliding interface.

1. Introduction

Inspection for fatigue cracks in cylindrically shaped components, such as the rotor hub of a helicopter, is an area of prime importance. Such components usually consist of (at least) an inner and outer cylinder, and these fatigue cracks usually form at the interface between these two layers; they then grow in the radial direction. Currently, detection of such radial cracks relies on visual inspection. The chief reasons that traditional ultrasonic techniques (such as pulse-echo) cannot be used to interrogate such a part, include problems associated with the curvature, the complicated nature of the reflected waveforms and accessibility difficulties. Therefore, it is desirable to develop more reliable, accurate and robust ultrasonic non-destructive methods to detect these cracks before catastrophic failure occurs.

* Corresponding author. Tel.: 001-404-894-5687; fax: 001-404-894-0186; e-mail: jianmin.qu@me.gatech.edu.

0020-7225/99/$ – see front matter
PII: S0020-7225(98)00133-5

A leading inspection candidate method is guided ultrasonic wave propagation; a guided wave propagates in the direction of the layer, while behaving as a standing wave through the thickness of the layer. These ultrasonic methodologies have the advantages of being remote, of using the geometry of the layered cylinder to their advantage, and of being well suited to real-time analysis. Guided waves have been commonly used to interrogate simple geometries such as beams and plates, but very little work has been done to generalize their applicability to layered cylinders. One such example is given by Nagy et al. [1], who suggested that radial fatigue cracks in weep holes in airframes may be detected by using guided waves propagating along the circumferential direction of the hole.

The motivation for this paper is the need to detect radial fatigue cracks in a shaft/bearing assembly (as shown in Fig. 1), using guided circumferential waves. Therefore, wave propagation in a layered cylinder must be understood. In order to accurately detect the crack, the dispersion relationship for guided circumferential waves must be known; this enables the selective generation of specific wave modes that carry the most energy to the interface (and to the crack).

Unfortunately, the solution to guided circumferential waves in a layered cylinder is not available. Most of the existing studies on cylindrical geometries focus on wave propagation in the axial direction of the cylinder. For example, wave propagation in a rod [2,3] and in a hollow cylinder [4,5] is well known; each of these papers concerns propagation of a guided wave in the axial direction of the cylinder. However, this paper addresses steady state, time harmonic guided wave propagation in the circumferential direction of a double layered cylinder (shaft/bearing

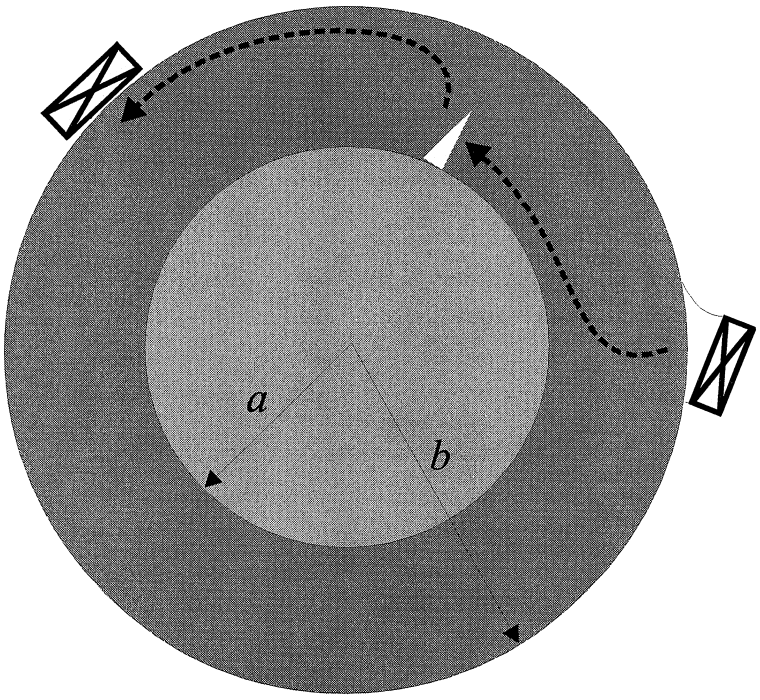

Fig. 1. Specimen geometry, and transducer interrogation.

assembly). The boundary condition at the interface (between the inner shaft and the outer cylinder) is assumed as free-sliding; that is, the interfacial shear stresses are assumed to be zero, and the normal stress and radial displacements are continuous. The dispersion relationship is obtained from linear elasticity theory and numerical results for the dispersion curves of the first several modes are presented. In addition, displacement profiles along the radial directions are provided.

Available work most relevant to the present study includes Qu et al. [6] and Liu and Qu [7], where the dispersion equation for guided circumferential waves in an annulus (hollow cylinder) is obtained, Liu and Qu [8], who examine transient waves propagating in the circumferential direction of an annulus subjected to an impulse load on its outer surface, and Kawald et al. [9], who look at circumferential surface waves on a thin layer over a solid cylinder.

This paper is arranged as follows: Section 2 introduces the boundary value problem for guided circumferential waves in a double layered cylinder; the method of solution for obtaining the dispersion curves is derived in Section 3; numerical results are presented in Section 4, including a discussion on the specific nature of the wave fields; and finally, conclusions are given in Section 5.

2. Problem statement

For steady-state, time harmonic waves in an isotropic, linearly elastic solid, the displacement equation of motion is given by

$$c_{\mathrm{L}}^2\nabla(\nabla\cdot\mathbf{u})-c_{\mathrm{T}}^2\nabla\times\nabla\times\mathbf{u}=\frac{\partial^2\mathbf{u}}{\partial t^2}, \tag{1}$$

where $\mathbf{u}$ is the displacement vector, c_{L} and c_{T} are the longitudinal and shear wave speeds, respectively,

$$c_{\mathrm{L}}^2=\frac{\lambda+2\mu}{\rho}, \tag{2a}$$

$$c_{\mathrm{T}}^2=\frac{\mu}{\rho}. \tag{2b}$$

In the above equations, ρ is the mass density, λ and μ are the Lamé constants.

Now, consider the cross-section of a layered cylinder as shown in Fig. 1. Assume that the cylinder is infinitely long in the axial direction. Therefore, for waves propagating in the circumferential direction, the assumptions of plane strain deformation prevail (two-dimensional linear elasticity theory). In this case, the pertinent non-zero displacement and stress components in a polar coordinate system $(r,\ \theta)$ are u_r, u_θ, σ_r, σ_θ and $\sigma_{r\theta}$. Spatially, these variables are all functions of r and θ only. It follows from [10] that the equation of motion (1) is identically satisfied if

$$u_r=\frac{\partial\varphi}{\partial r}+\frac{1}{r}\frac{\partial\psi}{\partial\theta}, \tag{3a}$$

$$u_\theta = \frac{1}{r}\frac{\partial \varphi}{\partial r} - \frac{\partial \psi}{\partial r}, \tag{3b}$$

where the potentials (φ and ψ) satisfy the wave equations

$$c_L^2 \nabla^2 \varphi = \frac{\partial^2 \varphi}{\partial t^2}, \tag{4a}$$

$$c_T^2 \nabla^2 \psi = \frac{\partial^2 \psi}{\partial t^2}. \tag{4b}$$

The corresponding stress components are related to the displacements through Hooke's law

$$\sigma_r = \lambda\left(\frac{\partial u_r}{\partial r} + \frac{u_r}{r} + \frac{1}{r}\frac{\partial u_\theta}{\partial \theta}\right) + 2\mu\frac{\partial u_r}{\partial r}, \tag{5a}$$

$$\sigma_{r\theta} = \mu\left(\frac{\partial u_\theta}{\partial r} - \frac{u_\theta}{r} + \frac{1}{r}\frac{\partial u_r}{\partial \theta}\right). \tag{5b}$$

To model the shaft/bearing assembly, the interface, $r = a$, between the inner shaft and the outer cylinder is assumed to be a free-sliding interface, i.e.

$$\sigma_{r\theta}(a + 0, \theta) = 0, \tag{6a}$$

$$\sigma_{r\theta}(a - 0, \theta) = 0, \tag{6b}$$

$$\sigma_r(a + 0, \theta) = \sigma_r(a - 0, \theta), \tag{7}$$

$$u_r(a + 0, \theta) = u_r(a - 0, \theta). \tag{8}$$

Furthermore, traction free boundary conditions are assumed on the outer surface, $r = b$, or

$$\sigma_r(b, \theta) = 0, \tag{9a}$$

$$\sigma_{r\theta}(b, \theta) = 0. \tag{9b}$$

Eqs. (3–9) form an eigenvalue problem. The solution of this eigenvalue problem gives the dispersion relationship between the wave number and the frequency (or phase velocity).

3. Method of solution

The expressions for the potentials of time harmonic waves propagating in the circumferential direction are

$$\varphi(\bar{r},\theta,t) = \Phi(\bar{r})\exp(\mathrm{i}\hat{k}\theta)\exp(-\mathrm{i}\omega t), \tag{10a}$$

$$\psi(\bar{r},\theta,t) = \Psi(\bar{r})\exp(\mathrm{i}\hat{k}\theta)\exp(-\mathrm{i}\omega t), \tag{10b}$$

where ω is the circular frequency and the non-dimensional variables are defined by

$$\bar{r} = \frac{r}{b}, \tag{11a}$$

$$\hat{k} = kb. \tag{11b}$$

The wave number k in Eq. (11b) is related to the phase velocity and circular frequency through

$$k = \frac{\omega}{c(b)}, \tag{12}$$

and $c(r)$ is the linear phase velocity for a material particle located at a distance r from the center of the inner shaft. In another form

$$c(\bar{r}) = \frac{\bar{\omega}}{\bar{k}}\frac{r}{b}c_{\mathrm{T}}, \tag{13}$$

where

$$\bar{\omega} = \frac{\omega h}{c_{\mathrm{T}}}, \tag{14a}$$

$$\bar{k} = kh, \tag{14b}$$

$$h = b - a. \tag{14c}$$

It can be easily shown that

$$\hat{k} = \frac{\bar{k}}{1-\eta}, \tag{15a}$$

$$\hat{\omega} = \frac{\hat{\omega}}{1-\eta}, \tag{15b}$$

where

$$\eta = \frac{a}{b}. \tag{15c}$$

It is important to note that the proposed model Eqs. (10a) and (10b) represents a guided wave that propagates in the direction of θ; this is accomplished by the term $\exp(\mathrm{i}\hat{k}\theta)$. This model was

first introduced by Viktorov [11] as the natural extension of Lamb waves, from plates to curved waveguides [12]. Viktorov's model is particularly well-suited for the current application, since the interrogation of a cylindrical component (such as a rotor hub) requires exciting waves that propagate in the circumferential direction. These waves would not be appropriate for interrogating *long* cylindrical components, such as piping; in this case, the wave of interest should propagate in the longitudinal direction [5]. In addition, the angular wave number (k in Eq. (11b)) in the current model is real (and not necessarily an integer). This implies that single-valueness for the potentials at 2π intervals is not necessarily satisfied (as opposed to the usual vibration model, where k must be an integer). However, this lack of single-valueness is not a problem, because the circumferential wave can be interpreted as traveling down a helix in the complex plane. As a result, a wave that travels a 2π interval, is not at the same starting location *in the complex plane*.

Substitution of (10) into (4) yields the solutions for the potentials

$$\Phi(\bar{r}) = \begin{cases} A_1 J_{\hat{k}}\left(\dfrac{\hat{\omega}\bar{r}}{\kappa}\right) + B_1 Y_{\hat{k}}\left(\dfrac{\hat{\omega}\bar{r}}{\kappa}\right), & \bar{r} > \eta, \\ A_2 J_{\hat{k}}\left(\dfrac{\hat{\omega}\bar{r}}{\kappa}\right), & \bar{r} < \eta, \end{cases} \tag{16}$$

$$\Psi(\bar{r}) = \begin{cases} C_1 J_{\hat{k}}\left(\hat{\omega}\bar{r}\right) + C_1 Y_{\hat{k}}\left(\hat{\omega}\bar{r}\right), & \bar{r} > \eta, \\ C_2 J_{\hat{k}}\left(\hat{\omega}\bar{r}\right), & \bar{r} < \eta, \end{cases} \tag{17}$$

where $J_{\hat{k}}(x)$ and $Y_{\hat{k}}(x)$ are the Bessel functions of the first and second kind, respectively. In the above equations,

$$\kappa = \frac{c_L}{c_T} = \frac{2(1-\nu)}{1-2\nu}, \tag{18}$$

with ν being the Poisson's ratio. Note that boundedness of the solution in the inner shaft implies the Bessel function of the second kind has to be discarded in that domain. The shaft (inner cylinder) is designated as material 2 and the bearing (outer cylinder) as material 1. The constants $\mathbf{A} = [A_1, B_1, C_1, D_1, A_2, C_2]^T$ are determined from the boundary conditions, (6–9).

Substituting Eqs. (16) and (17) into Eqs. (10a) and (10b), and then into (6–9) yields a system of six homogeneous equations for the six unknown constants, $\mathbf{A} = [A_1, B_1, C_1, D_1, A_2, C_2]^T$

$$[d_{ij}]\mathbf{A} = \mathbf{0}, \tag{19}$$

where elements of the 6×6 coefficient matrix of the system, $[d_{ij}]$, are functions of the dimensionless wave number, $\bar{k}$, and dimensionless frequency, $\bar{\omega}$, as well as the geometry parameter, η, and the Lamé constants of the two materials (λ and μ). These expressions are provided in Appendix A.

For non-trivial solutions, the determinant of matrix $[d_{ij}]$ must vanish, yielding

$$D(\bar{k}, \bar{\omega}) = \mathrm{Det}[d_{ij}] = 0. \tag{20}$$

This is the dispersion (characteristic) equation for circumferential waves in a layered cylinder. For each given $\bar{k}$, the dispersion Eq. (20) may have many roots for $\bar{\omega}$. As a result, the solution to Eq. (20) represents a family of curves, called modes. Each of these curves corresponds to a wave that propagates in the circumferential direction.

Once the dispersion Eq. (20) is solved, a non-zero eigenvector (up to an arbitrary multiplier), $\mathbf{A} = [A_1, B_1, C_1, D_1, A_2, C_2]^{\mathrm{T}}$ is determined from Eq. (19). This eigenvector is set to norm one without loss of generality. Substitution of the eigenvector (obtained from Eq. (19)) into Eqs. (16) and (17), then into Eqs. (10a) and (10b), and then finally into Eqs. (3a) and (3b), yields the displacement components of the circumferential wave

$$u_r(\bar{r}, \theta, t) = U_r(\bar{r}) \exp(\mathrm{i}\hat{k}\theta) \exp(-\mathrm{i}\omega t), \tag{21a}$$

$$u_\theta(\bar{r}, \theta, t) = U_\theta(\bar{r}) \exp(\mathrm{i}\hat{k}\theta) \exp(-\mathrm{i}\omega t), \tag{21b}$$

$$\begin{bmatrix} U_r(\bar{r}) \\ U_\theta(\bar{r}) \end{bmatrix} = \mathbf{W}(\bar{r})\mathbf{A}, \tag{22}$$

where $\mathbf{W}(\bar{r})$ is a 2×6 matrix whose elements are given in Appendix B.

4. Numerical results and discussion

This section provides numerical examples that illustrate some special features of guided circumferential waves in the layered cylinder (shown in Fig. 1). Since in the specific application of interest (rotor hub), the two parts are both made of steel, the materials in the layered cylinder are taken to be the same. The material properties and the geometry parameters used in the calculations are listed in Table 1.

For a given value of the non-dimensional wave number, $\bar{k}$, the dispersion Eq. (20) is solved numerically to obtain the corresponding non-dimensional frequency, $\bar{\omega}$. To this end, a bisection root-finding scheme is used. Care must be taken, since the value of the determinant changes very rapidly near its roots. For each given $\bar{k}$, Eq. (20) has an infinite number of real roots for $\bar{\omega}$. Each root corresponds to a propagating wave in the circumferential direction (a specific mode). After solving for all of the roots for various values of $\bar{k}$, the $\bar{\omega}$ versus $\bar{k}$ relationship is plotted graphically. These $\bar{\omega} - \bar{k}$ plots are called the dispersion curves.

Fig. 2 shows the dispersion curves for the first seven propagating modes. Note that at higher frequencies (higher wave number), all the curves become straight lines, illustrating that all modes become non-dispersive at high frequencies. In particular, the first mode becomes non-dispersive at

Table 1
Material and geometry data

ν	c_{T}	c_{L}	a	b	η
0.2817	3120 m/s	5660 m/s	5.08 cm	6.28 cm	0.8089

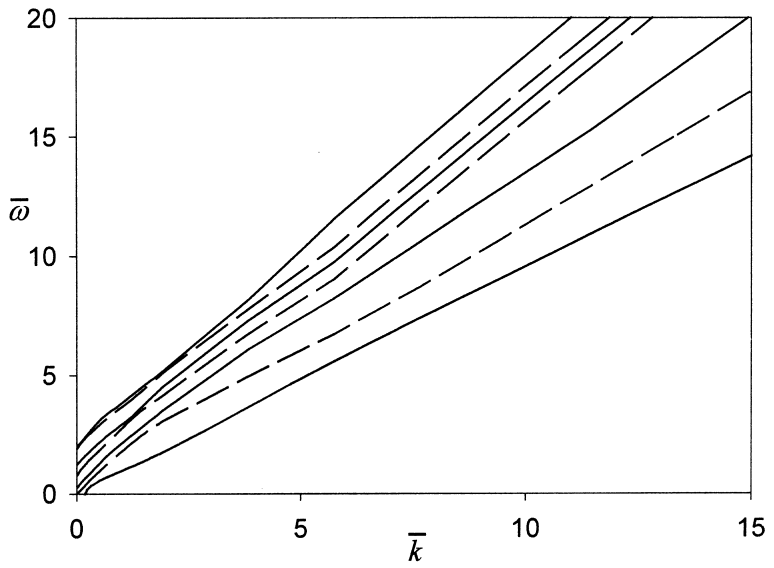

Fig. 2. The first seven branches of the dispersion curves for the double layered cylinder.

a fairly low frequency. It will be shown later that this first mode corresponds to the Rayleigh surface wave on the outer surface of the double layered cylinder.

To reveal the details of the solution at lower frequencies, the low frequency range of the dispersion curves for the first ten propagating modes are plotted in Fig. 3. It is seen from Fig. 3 that a cross-over point seems to occur between the 8th mode and the 9th mode. However, careful

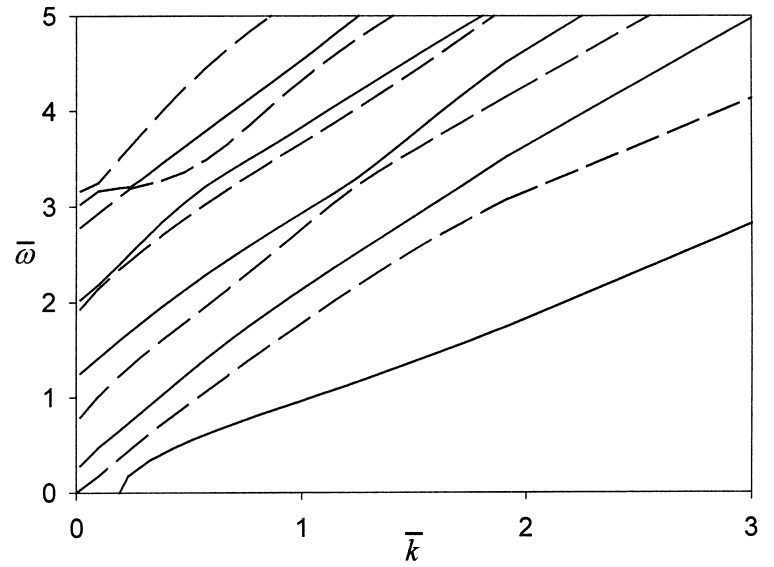

Fig. 3. A close-up at the low frequency of the first 10 branches of the dispersion curves for the double layered cylinder.

examination of the numerical results indicates that this is not the case. These two modes get very close, but do not touch each other. It is interesting to note that such cross-over does occur in the case of a hollow cylinder [7]. Physical interpretations of such cross-over phenomenon are also discussed in Ref. [7].

In order to investigate the effects of the "lubricant layer" and the "shaft/bearing" interactions, comparisons are made between three cases: a homogeneous solid cylinder of radius b; a hollow cylinder of inner radius a, outer radius b; and the layered cylinder shown in Fig. 1. The solutions to the solid and hollow cylinders are taken from [13] and [7], respectively.

For all three cases, the first mode corresponds to a surface wave on the outer surface of the cylinder. As the frequency tends to infinity (equivalently, as the radius of the cylinder tends to infinity), the outer surface can be viewed as a flat surface, and the first mode thus becomes the Rayleigh wave on a planar surface. For this reason, the fact that the cylinder is hollow or layered is irrelevant (for the first mode). Indeed, at higher frequencies, the dispersion curves for the first modes of each of these three cases approach a straight line, $\bar{\omega} = 0.9245\bar{k}$, which corresponds to the non-dispersive $\bar{\omega} - \bar{k}$ relationship for a Rayleigh wave on a planar surface (see Fig. 4(a)).

Fig. 4(b) demonstrates that the second modes show more dissimilarities among the three cases. These dissimilarities tend to disappear as the frequency increases. For the layered cylinder, the second mode behaves like an interface wave at higher frequencies. To illustrate this, the Stoneley wave velocity is calculated for a planar sliding interface between two isotropic elastic media (see Appendix C for the mathematical details). However, the calculations (in Appendix C) show this Stoneley wave is really an additional Rayleigh wave propagating at the free-sliding interface. For comparison purposes, the straight line pertinent to this case, $\bar{\omega} = 1.1216\bar{k}$, is also plotted in Fig. 4(b).

The higher modes have some interesting similarities among the three cases. As shown in Fig. 4(c)–(e), at low frequencies the homogeneous (solid) and the layered cylinders have very similar (in fact nearly identical) dispersion curves, whereas the hollow cylinder is markedly different. This is because the "lubricated" interface has very little effect at low frequencies. In contrast, at high frequencies, the homogeneous cylinder and the hollow cylinder are closer to one another (if not identical), whereas the layered cylinder clearly departs from the other two.

Next, consider the displacements. Once the dispersion equation (20) is solved, the eigenvector, $\mathbf{A}$, is determined (up to an arbitrary constant) from Eq. (19). For convenience, this eigenvector is normalized such that $\|\mathbf{A}\| = 1$. As previously mentioned, the numerical calculation of this coefficient vector is not a simple task. Care must be taken to calculate the root, the matrix and the eigenvector with very high precision (15 effective digits are used in these calculations). A singular value decomposition algorithm is also used to obtain a sufficiently accurate eigenvector, $\mathbf{A}$.

Once the eigenvector $\mathbf{A}$, has been calculated, the displacement components $U_r(\bar{r})$ and $U_\theta(\bar{r})$ are evaluated using Eq. (22). Furthermore, it follows from Eqs. (21a) and (21b) that the amplitude of the displacement vector can be computed as

$$U_n(\bar{r}) = \sqrt{|U_r(\bar{r})|^2 + |U_\theta(\bar{r})|^2}. \tag{23}$$

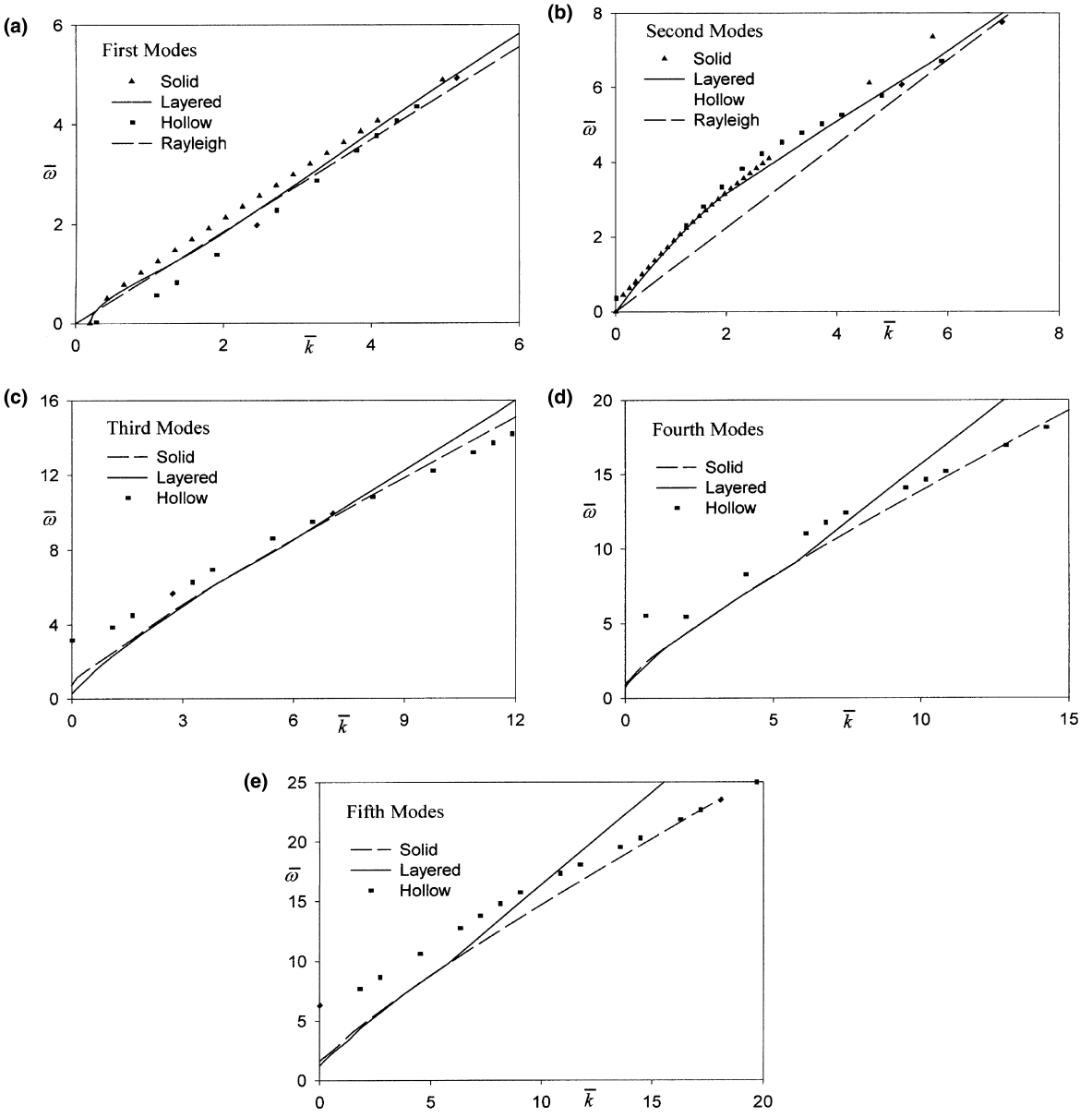

Fig. 4. (a) Comparison of the first mode among the solid, hollow, layered cylinders and the Rayleigh wave on the planar surface. (b) Comparison of the second mode among the solid, hollow, layered cylinders and the Rayleigh wave on the planar sliding-interface. (c) Comparison of the third mode among the solid, hollow, layered cylinders. (d) Comparison of the fourth mode among the solid, hollow, layered cylinders. (e) Comparison of the fifth mode among the solid, hollow, layered cylinders.

Because the amplitude of the eigenvector **A** is arbitrary, the amplitude of the displacement vector shown above Eq. (23) is normalized. For convenience, the displacements of each mode shown in the figures are normalized with respect to their maximum value along the entire radius, i.e.,

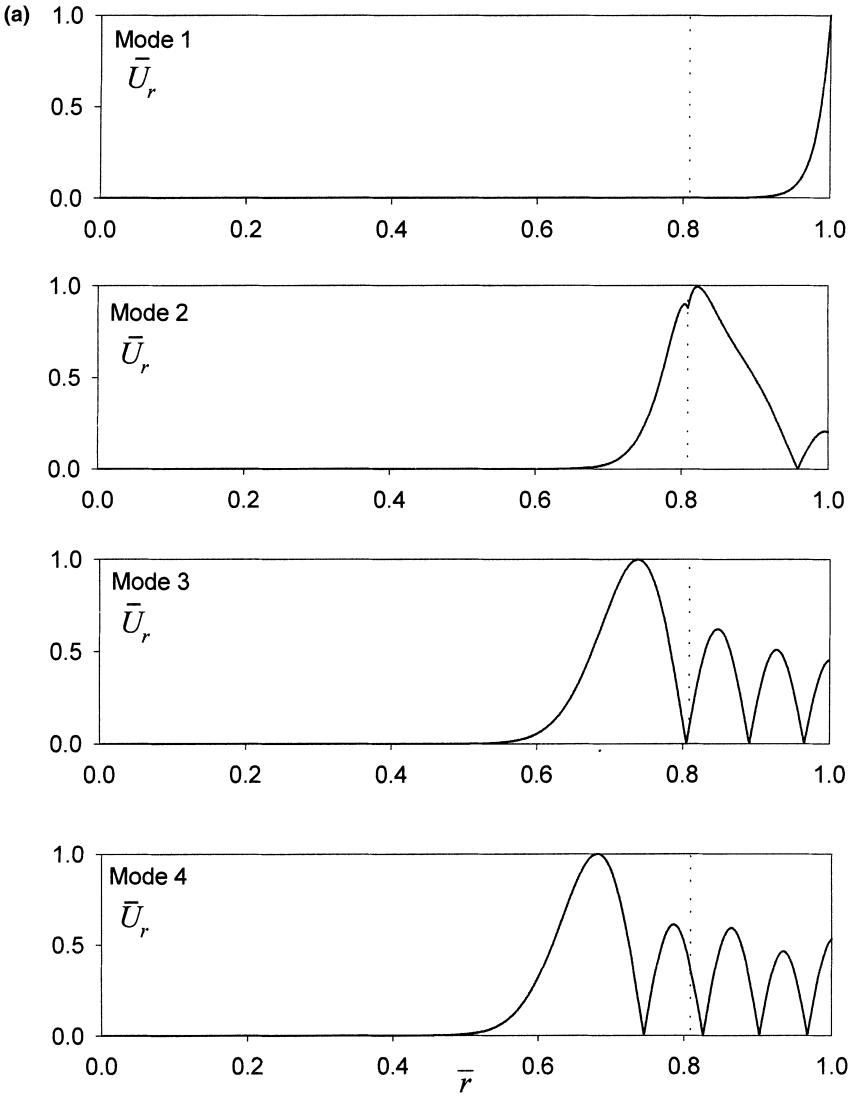

Fig. 5. (a) Normalized radial displacement distribution along the radial direction.

$$U_j(\bar{r}) = \frac{U_j(\bar{r})}{\max\{|U_j(\bar{r})|, \bar{r} \in [0,1]\}}, \quad j = r, \theta, n. \tag{24}$$

Note that the radial variation of the displacements given in Eq. (22) depends on the frequency through the eigenvalue Eq. (19). In the following numerical examples, the frequency is chosen as $\bar{\omega} = 63.23$ which corresponds to a real frequency of 0.5 MHz. The corresponding non-dimensional wave numbers are $\hat{k} = 66.48$, 56.04, 43.96, and 40.41, respectively, for the first four modes.

Variations of the displacement amplitude along the radial direction are shown in Fig. 5(a)–(c). The vertical dotted lines in the figures indicate the location of the shaft/bearing interface. First, it

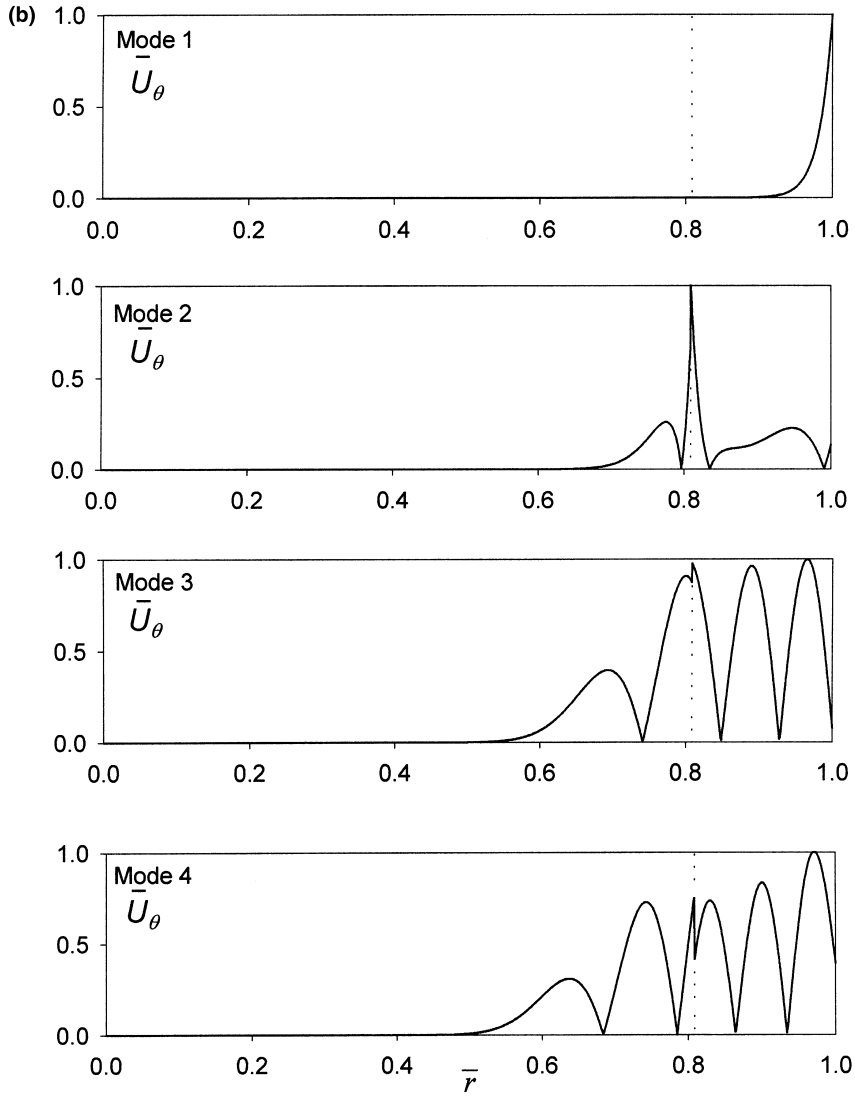

Fig. 5. (b) Normalized tangential displacement distribution along the radial direction.

is seen that higher modes have more nodal points. Furthermore, the radial displacement (Fig. 5(a)) is continuous, while the tangential displacement (Fig. 5(b)) is discontinuous due to the "lubricated" interfacial condition at the shaft/bearing interface. It can also be seen from Fig. 5(c) that, for the first mode, most of the energy is concentrated on the outer most surface (similar to a Rayleigh surface wave). As the mode number becomes larger, the energy concentration shifts progressively towards the center of cylinder.

The primary application of this work is to detect radial cracks growing from the interface between the two cylinders. The dispersion curves and displacement profiles developed in this study demonstrate that the second mode is most suitable for this application because its energy content is concentrated at the interface (at the frequency of interest, here 0.5 MHz). Therefore, the

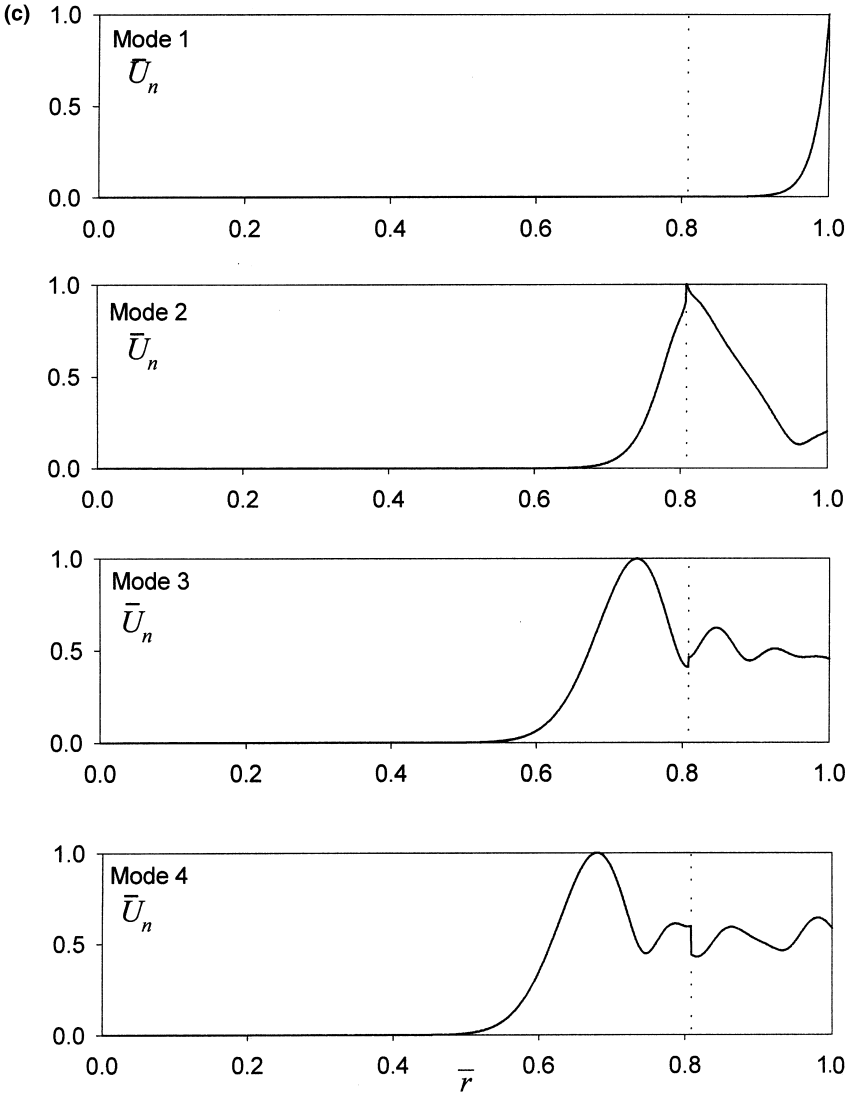

Fig. 5. (c) Normalized normal displacement amplitude distribution along the radial direction.

generation apparatus (transducers, for example) should be set up to preferentially launch this second (Rayleigh) mode, by applying the principle of matching trace velocity to determine the best insonification angle.

Before closing this section, it should be mentioned that the solution predicts an unbounded displacement field near the center, when $\bar{k} = kb < 1$. This is because in the displacement expression (22), there are terms like $J_{\hat{k}}(\hat{\omega}\bar{r}/\kappa)/\bar{r}$ which become unbounded as $\bar{r} \to 0$ for $\bar{k} < 1$ [14]. Note that $kb = 1$ corresponds to a wavelength equal to the outer circumference of the cylinder. It is obvious that for a wave to propagate in the circumferential direction, its wavelength must be less than the circumference. In other words, the assumption given in Eqs. (10a) and (10b) is valid only for waves with high enough frequencies such that $\hat{k} = kb > 1$. When the wavelength is less than

the circumference of the cylinder ($\hat{k} = kb > 1$), the type of circumferential waves defined in Eqs. (10a) and (10b) do not exist [15].

5. Conclusion

This paper examines the propagation of time harmonic circumferential waves in a two dimensional (infinitely long) hollow cylinder with an inner shaft. The boundary condition at the interface (between the inner shaft and the outer cylinder) is assumed as free-sliding; that is, the interfacial shear stresses are assumed to be zero, and the normal stress and radial displacements are continuous. For comparison purposes, results of circumferential waves in a homogeneous solid cylinder and a hollow cylinder are also presented. It is found that:

1. At low frequencies, circumferential waves in the layered cylinder behave very much like those in a homogeneous solid cylinder, whereas at high frequencies the dispersion curves of the layered cylinder are very different from those of both the solid and hollow cylinders.
2. At higher frequencies, the first mode tends asymptotically to a Rayleigh wave on a flat surface, while the second mode also approaches an additional Rayleigh wave that propagates along the sliding interface.
3. Circumferential waves do not exist when the wavelength is less than the circumference of the cylinder.

Acknowledgements

This work is supported by the Office of Naval Research M-URI Program "Integrated Diagnostics" (Contract number: N00014-95-1-0539). Two Amelia Earhart fellowships from the Zonta Foundation are also gratefully acknowledged.

Appendix A

Please note that for completeness, those coefficients are given for the general case of cylindrical layers made of different materials.

$$d_{11} = \left(2\frac{\mu_1}{\lambda_1}\hat{k}(\hat{k}-1) - \left(\frac{\hat{\omega}_1}{\kappa_1}\right)^2\left(1+2\frac{\mu_1}{\lambda_1}\right)\right)J_{\hat{k}}\left(\frac{\hat{\omega}_1}{\kappa_1}\right) + 2\frac{\hat{\omega}_1}{\kappa_1}\frac{\mu_1}{\lambda_1}J_{\hat{k}+1}\left(\frac{\hat{\omega}_1}{\kappa_1}\right),$$

$$d_{12} = \left(2\frac{\mu_1}{\lambda_1}\hat{k}(\hat{k}-1) - \left(\frac{\hat{k}_1}{\kappa_1}\right)^2\left(1+2\frac{\mu_1}{\lambda_1}\right)\right)Y_{\hat{k}}\left(\frac{\hat{\omega}_1}{K_1}\right) + 2\frac{\hat{\omega}_1}{\kappa_1}\frac{\mu_1}{\lambda_1}Y_{\hat{k}+1}\left(\frac{\hat{\omega}_1}{\kappa_1}\right),$$

$$d_{13} = 2\frac{\mu_1}{\lambda_1}i\hat{k}((\hat{k}-1)J_{\hat{k}}(\hat{\omega}_1) - \hat{\omega}_1 J_{\hat{k}+1}(\hat{\omega}_1)),$$

$$d_{14} = 2\frac{\mu_1}{\lambda_1} i\hat{k}((\hat{k}-1)Y_{\hat{k}}(\hat{\omega}_1) - \hat{\omega}_1 Y_{1\hat{k}+1}(\hat{\omega}_1)),$$

$$d_{15} = 0, \quad d_{16} = 0,$$

$$d_{21} = 2i\hat{k}\left((\hat{k}-1)J_{\hat{k}}\left(\frac{\hat{\omega}_1}{\kappa_1}\right) - \frac{\hat{\omega}_1}{\kappa_1}J_{\hat{k}+1}\left(\frac{\hat{\omega}_1}{\kappa_1}\right)\right),$$

$$d_{22} = 2i\hat{k}\left((\hat{k}-1)Y_{\hat{k}}\left(\frac{\hat{\omega}_1}{\kappa_1}\right) - \frac{\hat{\omega}_1}{\kappa_1}Y_{\hat{k}+1}\left(\frac{\hat{\omega}_1}{\kappa_1}\right)\right),$$

$$d_{23} = (\hat{\omega}_1^2 - 2\hat{k}(\hat{k}-1))J_{\hat{k}}(\hat{\omega}_1) - 2\hat{\omega}_1 J_{\hat{k}+1}(\hat{\omega}_1),$$

$$d_{24} = (\hat{\omega}_1^2 - 2\hat{k}(\hat{k}-1))Y_{\hat{k}}(\hat{\omega}_1) - 2\hat{\omega}_1 Y_{\hat{k}+1}(\hat{\omega}_1),$$

$$d_{25} = 0, \quad d_{26} = 0,$$

$$d_{31} = \left(2\frac{\mu_1}{\lambda_1\eta^2}\hat{k}(\hat{k}-1) - \left(\frac{\hat{\omega}_1}{\kappa_1}\right)^2\left(1+2\frac{\mu_1}{\lambda_1}\right)\right)J_{\hat{k}}\left(\frac{\hat{\omega}_1\eta}{\kappa_1}\right) + 2\frac{\hat{\omega}_1}{\kappa_1\eta}\frac{\mu_1}{\lambda_1}J_{\hat{k}+1}\left(\frac{\hat{\omega}_1\eta}{\kappa_1}\right),$$

$$d_{32} = \left(2\frac{\mu_1}{\lambda_1\eta^2}\hat{k}(\hat{k}-1) - \left(\frac{\hat{k}}{\kappa_1}\right)^2\left(1+2\frac{\mu_1}{\lambda_1}\right)\right)Y_{\hat{k}}\left(\frac{\hat{\omega}_1\eta}{\kappa_1}\right) + 2\frac{\hat{\omega}_1}{\kappa_1\eta}\frac{\mu_1}{\lambda_1}Y_{\hat{k}+1}\left(\frac{\hat{\omega}_1\eta}{\kappa_1}\right),$$

$$d_{33} = 2\frac{\mu_1}{\lambda_1\eta} i\hat{k}\left(\frac{\hat{k}-1}{\eta}J_{\hat{k}}(\hat{\omega}_1\eta) - \hat{\omega}_1 J_{\hat{k}+1}(\hat{\omega}_1\eta)\right),$$

$$d_{34} = 2\frac{\mu_1}{\lambda_1\eta} i\hat{k}\left(\frac{\hat{k}-1}{\eta}Y_{\hat{k}}(\hat{\omega}_1\eta) - \hat{\omega}_1 Y_{\hat{k}+1}(\hat{\omega}_1\eta)\right),$$

$$d_{35} = -\left(\left(2\frac{\mu_2}{\lambda_1\eta^2}\hat{k}(\hat{k}-1) - \left(\frac{\hat{\omega}_2}{\kappa_2}\right)^2\left(\frac{\lambda_2}{\lambda_1}+2\frac{\mu_2}{\lambda_1}\right)\right)J_{\hat{k}}\left(\frac{\hat{\omega}_2\eta}{\kappa_2}\right) + 2\frac{\hat{\omega}_2}{\kappa_2\eta}\frac{\mu_2}{\lambda_1}J_{\hat{k}+1}\left(\frac{\hat{\omega}_2\eta}{\kappa_2}\right)\right),$$

$$d_{36} = -2\frac{\mu_2}{\lambda_1\eta} i\hat{k}\left(\frac{\hat{k}-1}{\eta}J_{\hat{k}}(\hat{\omega}_2\eta) + \hat{\omega}_2 J_{\hat{k}+1}(\hat{\omega}_2\eta)\right),$$

$$d_{41} = 2i\frac{\hat{k}}{\eta}\left(\frac{\hat{k}-1}{\eta}J_{\hat{k}}\left(\frac{\hat{\omega}_1\eta}{\kappa_1}\right) - \frac{\hat{\omega}_1}{\kappa_1}J_{\hat{k}+1}\left(\frac{\hat{\omega}_1\eta}{\kappa_1}\right)\right),$$

$$d_{42} = 2i\frac{\hat{k}}{\eta}\left(\frac{\hat{k}-1}{\eta}Y_{\hat{k}}\left(\frac{\hat{\omega}_1\eta}{\kappa_1}\right) - \frac{\hat{\omega}_1}{\kappa_1}Y_{\hat{k}+1}\left(\frac{\hat{\omega}_1\eta}{\kappa_1}\right)\right),$$

$$d_{43} = \left(\hat{\omega}_1^2 - (\hat{k}-1)\frac{2\hat{k}}{\eta^2}\right)J_{\hat{k}}(\hat{\omega}_1\eta) - \frac{2\hat{\omega}_1}{\eta}J_{\hat{k}+1}(\hat{\omega}_1\eta),$$

$$d_{44} = \left(\hat{\omega}_1^2 - (\hat{k}-1)\frac{2\hat{k}}{\eta^2}\right)Y_{\hat{k}}(\hat{\omega}_1\eta) - \frac{2\hat{\omega}_1}{\eta}Y_{\hat{k}+1}(\hat{\omega}_1\eta),$$

$$d_{45} = 0, \quad d_{46} = 0, \quad d_{51} = 0, \quad d_{52} = 0, \quad d_{53} = 0, \quad d_{54} = 0,$$

$$d_{55} = 2i\frac{\hat{k}}{\eta}\left(\frac{\hat{k}-1}{\eta}J_{\hat{k}}\left(\frac{\hat{\omega}_2\eta}{\kappa_2}\right) - \frac{\hat{\omega}_2}{\kappa_2}J_{\hat{k}+1}\left(\frac{\hat{\omega}_2\eta}{\kappa_2}\right)\right),$$

$$d_{56} = \left(\hat{\omega}_2^2 - (\hat{k}-1)\frac{2\hat{k}}{\eta^2}\right)J_{\hat{k}}(\hat{\omega}_2\eta) - \frac{2\hat{\omega}_2}{\eta}J_{\hat{k}+1}(\hat{\omega}_2\eta),$$

$$d_{61} = \hat{k}J_{\hat{k}}\left(\frac{\hat{\omega}_1\eta}{\kappa_1}\right) - \frac{\hat{\omega}_1\eta}{\kappa_1}J_{\hat{k}+1}\left(\frac{\hat{\omega}_1\eta}{\kappa_1}\right),$$

$$d_{62} = \hat{k}Y_{\hat{k}}\left(\frac{\hat{\omega}_1\eta}{\kappa_1}\right) - \frac{\hat{\omega}_1\eta}{\kappa_1}Y_{\hat{k}+1}\left(\frac{\hat{\omega}_1\eta}{\kappa_1}\right),$$

$$d_{63} = i\hat{k}J_{\hat{k}}(\hat{\omega}_1\eta),$$

$$d_{64} = i\hat{k}Y_{\hat{k}}(\hat{\omega}_1\eta),$$

$$d_{65} = \frac{\hat{\omega}_2\eta}{\kappa_2}J_{\hat{k}+1}\left(\frac{\hat{\omega}_2\eta}{\kappa_2}\right) - \hat{k}J_{\hat{k}}\left(\frac{\hat{\omega}_2\eta}{\kappa_2}\right),$$

$$d_{66} = -i\hat{k}J_{\hat{k}}(\hat{\omega}_2\eta),$$

where

$$\kappa_1 = \frac{c_{\mathrm{L}}^{(1)}}{c_{\mathrm{T}}^{(1)}}, \quad \kappa_2 = \frac{c_{\mathrm{L}}^{(2)}}{c_{\mathrm{T}}^{(2)}}, \quad \hat{\omega}_2 = \frac{\omega b}{c_{\mathrm{T}}^{(2)}}, \quad \hat{\omega}_1 = \frac{\omega b}{c_{\mathrm{T}}^{(1)}},$$

λ_1 and μ_1 are the material constants of medium 1,
λ_2 and μ_2 are the material constants of medium 2.

Appendix B

Please note that for completeness, those coefficients are given for the general case of cylindrical layers made of different materials.

For $0 \leqslant \bar{r} \leqslant \eta$,

$$W_{11} = W_{12} = W_{13} = W_{14} = 0,$$

$$W_{15} = \frac{\hat{k}}{\bar{r}} J_{\hat{k}}\left(\frac{\hat{\omega}_2}{\kappa_2}\bar{r}\right) - \frac{\hat{\omega}_2}{\kappa_2} J_{\hat{k}+1}\left(\frac{\hat{\omega}_2}{\kappa_2}\bar{r}\right),$$

$$W_{16} = i\frac{\hat{k}}{\bar{r}} J_{\hat{k}}(\hat{\omega}_2\bar{r}),$$

$$W_{21} = W_{22} = W_{23} = W_{24} = 0,$$

$$W_{25} = i\frac{\hat{k}}{\bar{r}} J_{\hat{k}}\left(\frac{\hat{\omega}_2}{\kappa_2}\bar{r}\right),$$

$$W_{26} = -\frac{\hat{k}}{\bar{r}} J_{\hat{k}}(\hat{\omega}_2\bar{r}) + \hat{\omega}_2 J_{\hat{k}+1}(\hat{\omega}_2\bar{r}).$$

For $\eta \leqslant \bar{r} \leqslant 1$,

$$W_{11} = \frac{\hat{k}}{\bar{r}} J_{\hat{k}}\left(\frac{\hat{\omega}_1}{\kappa_1}\bar{r}\right) - \frac{\hat{\omega}_1}{\kappa_1} J_{\hat{k}+1}\left(\frac{\hat{\omega}_1}{\kappa_1}\bar{r}\right),$$

$$W_{12} = \frac{\hat{k}}{\bar{r}} Y_{\hat{k}}\left(\frac{\hat{\omega}_1}{\kappa_1}\bar{r}\right) - \frac{\hat{\omega}_1}{\kappa_1} Y_{\hat{k}+1}\left(\frac{\hat{\omega}_1}{\kappa_1}\bar{r}\right),$$

$$W_{13} = i\frac{\hat{k}}{\bar{r}}J_{\hat{k}}(\hat{\omega}_1\bar{r}),$$

$$W_{14} = i\frac{\hat{k}}{\bar{r}}J_{\hat{k}}(\hat{\omega}_1\bar{r}),$$

$$W_{15} = W_{16} = 0,$$

$$W_{21} = i\frac{\hat{k}}{\bar{r}}J_{\hat{k}}\left(\frac{\hat{\omega}_1}{\kappa_1}\bar{r}\right),$$

$$W_{22} = i\frac{\hat{k}}{\bar{r}}Y_{\hat{k}}\left(\frac{\hat{\omega}_1}{\kappa_1}\bar{r}\right),$$

$$W_{23} = -\frac{\hat{k}}{\bar{r}}J_{\hat{k}}(\hat{\omega}_1\bar{r}) + \hat{\omega}_1 J_{\hat{k}+1}(\hat{\omega}_1\bar{r}),$$

$$W_{24} = -\frac{\hat{k}}{\bar{r}}Y_{\hat{k}}(\hat{\omega}_1\bar{r}) + \hat{\omega}_1 Y_{\hat{k}+1}(\hat{\omega}_1\bar{r}),$$

$$W_{25} = W_{26} = 0.$$

Appendix C

An interfacial wave that propagates along a planar interface between two elastic media is called a Stoneley wave. The amplitude of a Stoneley wave decays exponentially away from the interface, so most of the energy is concentrated along the interface. This Appendix considers a Stoneley wave on a sliding interface between two elastic solids. The procedure was explained and derived in Ref. [16]. This paper shows that the characteristic equation when the materials on the two sides of the interface are the same is,

$$\begin{vmatrix} \frac{b_1}{k} & \frac{k}{b_2} & \frac{b_1}{k} & \frac{k}{b_2} \\ 2\frac{b_1}{k} & \left(2-\frac{c^2}{c_T^2}\right)\frac{k}{b_2} & 0 & 0 \\ 0 & 0 & 2\frac{b_1}{k} & \left(2-\frac{c^2}{c_T^2}\right)\frac{k}{b_2} \\ 2-\frac{c^2}{c_T^2} & 2 & -2+\frac{c^2}{c_T^2} & -2 \end{vmatrix} = 0, \tag{C.1}$$

where

$$b_1 = k\left(1 - \frac{c^2}{c_L^2}\right)^{1/2} \tag{C.2a}$$

$$b_2 = k\left(1 - \frac{c^2}{c_T^2}\right)^{1/2}, \tag{C.2b}$$

It is easy to verify that this equation does not involve the wave number k as expected since the Stoneley wave on a planar interface is non-dispersive. Additionally, it can be shown that Eq. (C.1) reduces to

$$R(c_L, c_T, c)\left(1 - \frac{c^2}{c_L^2}\right)^{1/2} = 0, \tag{C.3}$$

where $R(c_L, c_T, c)$ is the Rayleigh surface wave equation [10]. Therefore, the free-sliding interface does not support a Stoneley wave at all, but only an additional Rayleigh wave propagating at the interface. The authors also found that a frictional interface does not support a Stoneley wave.

References

[1] P.B. Nagy, M. Blodgett, M. Godis, Weep hole inspection by circumferential creeping waves, NDT and E International 27 (1994) 131–142.
[2] R.D. Mindlin, Axially symmetric waves in elastic rods, J. Appl. Mech. 82 (1960a) 145–151.
[3] R.D. Mindlin, H.D. McNiven, Axially symmetric waves in elastic rods, J. Appl. Mech. 82 (1960b) 145–151.
[4] D. Gazis, I. Three dimensional investigation of the propagation of waves in hollow circular cylinders, Analytical foundation, II. Numerical results, J. Acoust. Soc. Am. 31–35 (1959) 568–578.
[5] J.L. Rose, J.J. Ditri, A. Pilarski, K. Rajana, F. Carr, A guided wave inspection technique for nuclear steam generator tubing, NDT and E International 27 (6) (1994) 307–310.
[6] J. Qu, Y. Berthelot, Z. Li, Dispersion of guided circumferential waves in circular annulus, Review of Progress in Quantitative NDE 15A (1996) 169–176.
[7] G. Liu, J. Qu, Guided circumferential waves in a circular annulus, J. Appl. Mech. 65 (1998) 424–430.
[8] G. Liu, J. Qu, Transient wave propagation in a circular annulus subjected to impulse excitation on its outer surface, J. Acoust. Soc. Amer. 103 (3) (1998) 1210–1220.
[9] U. Kawald, C. Desmet, W. Lauriks, C. Glorieux, J. Thoen, Investigation of the dispersion relations of surface acoustic waves propagating on a layered cylinder, J. Acoust. Soc. Amer. 99 (2) (1996) 926–930.
[10] J.D. Achenbach, Wave Propagation in Elastic Solids, North-Holland, New York, 1984.
[11] I.A. Viktorov, Rayleigh-type waves on curved surfaces, J. Acoust. Soc. Am. 4 (1958) 131–136.
[12] I.A. Viktorov, Rayleigh and Lamb Waves, Plenum Press, New York, 1967.
[13] J. Cerv, Dispersion of elastic waves and Rayleigh-type waves in a thin disc, Acta Technica Csav 1 (1988) 89–99.
[14] M. Abramowitz, I.A. Stegun, Handbook of Mathematical Functions, Dover, New York, 1965.
[15] C. Valle, Guided circumferential waves in layered annular structures, Ph.D. Thesis, G.W. Woodruff School of Mechanical Engineering, Georgia Institute of Technology, 1999.
[16] J.D. Achenbach, H.I. Epstein, Dynamic interaction of a layer and a half-space, in: Proceedings of the American Society of Civil Engineers, Journal of the Engineering Mechanics Division, vol. 93, EM5, 1967, pp. 27–42 .